Ellipsoidal Coulomb crystals in a linear radio-frequency trap

U. Fröhlich, B. Roth, and S. Schiller
Institut für Experimentalphysik, Heinrich-Heine-Universität Düsseldorf, 40225 Düsseldorf, Germany

(Received 17 March 2005; accepted 1 June 2005; published online 1 July 2005)

A static quadrupole potential breaks the cylindrical symmetry of the effective potential of a linear rf trap. For a one-component liquid plasma at low temperature, the resulting equilibrium charge distribution is predicted to be an ellipsoid. Laser-cooled $^9Be^+$ ellipsoidal ion crystals were produced and good agreement was found between their shapes and the cold fluid prediction. In two-species mixtures, containing $^9Be^+$ and sympathetically cooled ions of lower mass, a sufficiently strong static quadrupole potential produces a complete spatial separation of the species. © *2005 American Institute of Physics*. [DOI: 10.1063/1.1976605]

I. INTRODUCTION

One-component plasmas have attracted significant attention in the past since they represent simple multiparticle systems that can be studied under a variety of conditions with a high degree of experimental control. Detailed theoretical analysis, both by analytical and by molecular dynamics (MD) simulations, is possible.[1,2]

To overcome the Coulomb repulsion, the plasmas are confined in Penning- or Paul-type traps. Their temperature can be varied over many orders of magnitude. In particular, they can be efficiently cooled to the millikelvin range by laser cooling. Strong cooling results in phase transitions to a crystalline state, whose occurrence is described by the interaction parameter $\Gamma = Q^2/4\pi\epsilon_0 a k_B T$, the ratio between average nearest-neighbor Coulomb energy and thermal energy (a, average particle spacing; Q, particle charge). The MD simulations on infinite systems have shown that the plasma becomes liquidlike, i.e., exhibits spatial correlations for $\Gamma \geqslant 2$, without going through a discontinuous gas-liquid phase transition.[2] For $\Gamma > 170$ (Ref. 3) a phase transition to a crystal occurs. Coulomb crystals in hyperbolic[4] and linear Paul (rf) traps[5,6] have become of great importance in quantum optics, where they can be used to implement quantum gates or quantum memories[7] and can serve as systems for precision measurements on atomic or molecular ions.[8,9]

The spatial distribution of a trapped one-component gaseous plasma differs significantly from the liquid and crystalline state. This is described by Debye length $\lambda_D = (k_B T \epsilon_0 / n Q^2)^{1/2}$, which is the distance below which interactions between individual particles overcome collective effects.[2] Here, n is the particle density of the plasma. When λ_D is much larger than the spatial extent of the plasma, the Coulomb interaction is negligible, and the density is a local function of the trap potential only. For a harmonic potential, the density then has a Gaussian dependence on the coordinates, with plasma dimensions inversely proportional to the respective trap potential curvatures. When λ_D is comparable to or smaller than the spatial extent of the plasma (as is the case for the plasmas presented in this paper), space charge becomes important.[10] The density is then a local function of both trap potential and space charge potential. Since the latter depends on the density distribution over the whole space, a self-consistent density distribution arises, whose shape exhibits a nontrivial dependence on the trap potential curvatures. For cylindrical trap potential symmetry, such plasmas are spheroids (ellipses of revolution) and have been studied both in linear rf and Penning traps.[11,12] In the absence of cylindrical symmetry the shape has been predicted to be that of an ellipsoid.[13] Ellipsoidal plasmas have already been observed and studied in Penning traps (see Ref. 14, and references therein). In this study we describe the observation and characterization of cold ellipsoidal plasmas in a linear rf trap. In particular, we have obtained ellipsoidal crystals containing two different ion species.

II. LINEAR PAUL TRAP

The linear rf trap used in this experiment consists of four rods of radius r' (inset in Fig. 2), each divided into three electrically isolated segments. A radio-frequency voltage $V_{rf}\sin \Omega t$ and a static voltage V_{DC} are applied to the rods in a quadrupolar configuration. Confinement along the trap axis (z axis) is achieved by raising the two end segments of each rod by a static voltage V_{EC}. When the Mathieu stability parameter $q = 2QV_{rf}/mr_0^2\Omega^2 \ll 1$, the independent motion of the trapped ions (mass m) can be adequately described by the motion in a harmonic effective potential (pseudopotential) $U_{\text{trap}}(\mathbf{r}) = m\Sigma\omega_i^2 x_i^2/2$,[15] and an additional jitter motion at the radio frequency Ω, the so-called micromotion. r_0 is the minimum distance from the electrode surfaces to the trap axis. The axial (ω_z) and transverse (ω_x and ω_y) frequencies of the effective trap potential are given by $\omega_z^2 = 2\kappa Q V_{EC}/m$ and $\omega_{x,y}^2 = Q^2 V_{rf}^2/(2m^2\Omega^2 r_0^4) - \omega_z^2/2 \pm QV_{DC}/mr_0^2$, where κ is a constant determined by the trap geometry. For vanishing static voltage V_{DC}, ω_x and ω_y are degenerate. With the application of a static voltage $V_{DC} \neq 0$, a static quadrupole potential is added to the effective trap potential, and the cylindrical symmetry is broken. The transverse trap frequencies ω_x and ω_y increase and decrease, respectively, until ω_y vanishes for a sufficiently large applied voltage V_{DC}, which implies that the ion motion along the y direction becomes unstable.

III. THEORETICAL DESCRIPTION

In the liquid phase, a trapped plasma in thermal equilibrium at a given temperature T may be regarded as a macroscopic charged fluid with number density $n_f(\mathbf{r})$.[2,16] For example, this description leads to an expression for the equilibrium shape of the trapped plasma. A particularly simple analytical treatment is possible in the limit of an ultracold plasma when $T \to 0$. In this case, the equilibrium number density $n_f(\mathbf{r})$ is determined by the condition of no net force on any plasma region. However, at very low temperatures, the plasma does not remain liquid but crystallizes with the appearance of shells and a fairly complicated structure. While the fluid description may be expected to become inaccurate in this case, it has been shown to remain applicable as far as the shape of the outer boundary is concerned and as long as the crystals are sufficiently large. For linear rf traps, this comparison has so far only been performed for the case of cylindrical symmetry ($V_{DC}=0$).[11]

In the effective potential approximation, the absence of net force implies a balance between the electric field due to the space charge potential $\phi_f(\mathbf{r})$ and the trap force due to the effective potential: $Q\phi_f(\mathbf{r})+U_{\text{trap}}(\mathbf{r})=\text{const}$. The number density follows directly from Poisson's equation, $n_f(\mathbf{r}) = (\epsilon_0/Q^2)\Delta U_{\text{trap}}(\mathbf{r})$. For the harmonic effective potential of the linear rf trap with the above trap frequencies the number density is explicitly given by $n_0=\epsilon_0 V_{rf}^2/m\Omega^2 r_0^4$, which is constant within the fluid and independent of the static voltages V_{DC} and V_{EC}.

The outer shape of the zero-temperature charged fluid with constant number density is an ellipsoid with principal axes R_x, R_y, and L in the x, y, and z directions, respectively.[13] With the additional boundary condition that the electric space charge potential $\phi_f(\mathbf{r})$ vanishes at infinity, the potential inside the fluid is given by

$$\phi_f(\mathbf{r}) = \frac{Qn_0}{4\epsilon_0}[A_x(R_x^2 - x^2) + A_y(R_y^2 - y^2) + A_z(L^2 - z^2)], \tag{1}$$

where the dimensionless functions A_x, A_y, and A_z depend on the principal axes R_x, R_y, and L, respectively.[13] Force balance implies that A_i satisfies $\omega_i^2 = Q^2 n_0 A_i/2m\epsilon_0$. The ratios of the principal axes R_x/L and R_y/L can thus be calculated by solving the set of equations

$$\left(\frac{\omega_x}{\omega_z}\right)^2 = \frac{A_x(R_x/L, R_y/L)}{A_z(R_x/L, R_y/L)},$$

$$\left(\frac{\omega_y}{\omega_z}\right)^2 = \frac{A_y(R_x/L, R_y/L)}{A_z(R_x/L, R_y/L)}. \tag{2}$$

For $V_{DC}=0$, ω_x and ω_y are equal, and the equilibrium shape of the zero-temperature charged fluid is a spheroid with radius $R=R_x=R_y$ and half length L. The two equations (2) then reduce to a single equation for the aspect ratio R/L. Hornekær *et al.*[11,17] have found good agreement between this theory and experimental aspect ratios of a large variety of spheroidal $^{40}Ca^+$ ion crystals, obtained by varying the endcap voltage V_{EC} and the radio-frequency amplitude V_{rf}.

IV. EXPERIMENT

We have tested the predictions of the charged fluid model in a fully anisotropic effective trap potential using a laser-cooled $^9Be^+$ ensemble. The linear trap properties were $r_0=4.32$ mm and a radio frequency $\Omega/2\pi=14.2$ MHz with an amplitude $V_{rf}=380$ V. This resulted in a small Mathieu stability parameter of $q=0.055$, implying that the micromotion was relatively small and that the effective potential description is appropriate. For axial confinement, $V_{EC}=4.5$ V was applied to the trap end segments, giving rise to $\kappa=3.0\times10^{-3}/\text{mm}^2$, an axial frequency of $\omega_z=2\pi\times85$ kHz, and a transverse frequency of $\omega_r=2\pi\times268$ kHz. Experimentally, both values were obtained from a measurement of the transverse frequency as a function of V_{EC}, in the absence of V_{DC}. This was done by external excitation of the radial motion of gas phase $^9Be^+$ ions in the harmonic trap potential, which was detected by a drop of the fluorescence signal from the laser cooled $^9Be^+$ ions.[18]

When the effective trap potential is made anisotropic by the application of V_{DC}, the predicted instability limit is 4.96 V. We observe partial particle loss when V_{DC} exceeds 4.2 V and total loss at $V_{DC}=4.9$ V. To prevent particle loss, we limited V_{DC} to a maximum of 4.2 V, corresponding to an increase of the transverse trap frequency $\omega_x/2\pi$ from 268 kHz to 365 kHz and a decrease of $\omega_y/2\pi$ from 268 kHz to 104 kHz. Experimentally, the two transverse frequencies ω_x and ω_y can be measured by secular excitation.

The trap was loaded with $^9Be^+$ ions by evaporating beryllium atoms from an oven and ionizing them in the trap center by electron impact. The trapped $^9Be^+$ ions, initially forming a hot plasma cloud of ≈1000 K, were laser cooled by laser radiation at 313 nm until they finally underwent a phase transition to a crystalline state with a temperature of a few millikelvin. A description of the all-solid-state laser system is given in Ref. 19. To image the $^9Be^+$ ion crystals, a charge-coupled device (CCD) camera was placed transverse to the trap axis.

V. RESULTS

Figure 1 shows an ion crystal containing $\simeq2\times10^3$ $^9Be^+$, at different values of V_{DC}. The estimate of the ion number in Fig. 1(a) is obtained from MD simulations in which the observed structure (especially the number of shells) is reproduced.[20] For the test of the calibration of the CCD optics magnification as well as the determination of absolute dimensions of the ion plasmas, we also use the MD simulations. As a check, multiplying the volume $4\pi R_{45}^2 L/3$ of the crystal shown in Fig. 1(a) and the cold fluid model density n_0, we obtain the value $\simeq2\times10^3$. This agrees well with the MD results and implies that the model is applicable for large crystals. The left central part of the ion crystal shown in Fig. 1(a) contains a dark region, which consists of sympathetically cooled ions originating from the residual gas and having a mass smaller than that of $^9Be^+$, pushed to one side by radiation pressure.[21]

In the outer region of the crystal shown in Fig. 1, the ions are arranged in concentric shells while the inner region is smeared out. The size of the smeared out region appears to

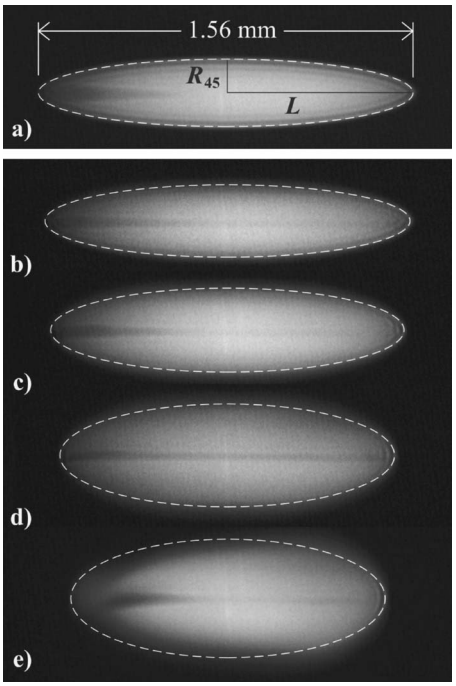

FIG. 1. CCD images of a large ion crystal containing $\simeq 2\times 10^3$ $^9Be^+$, taken perpendicular to the z axis and at 45 ° to the x and y axes, for different values of V_{DC}. Dashed lines, fits of ellipses with principal axes R_{45} and L to the outermost shells. (a) $V_{DC}=0$, the effective trap potential has cylindrical symmetry. The ion crystal is a prolate spheroid with radius $R_x=R_y=R_{45}$ and half length L. The aspect ratio $R_{45}/L=0.178$. (b)–(e) $V_{DC}\neq 0$, the cylindrical symmetry is broken and the crystal is an ellipsoid with principal axes $R_x<R_{45}$, $R_y>R_{45}$ and L. With increasing V_{DC} the crystal expands in the y direction and compresses in the x and z directions, while maintaining the constant volume. V_{DC} is set to 1.8 (b), 2.8 (c), 3.6 (d), and 4.2 V (e), leading to an aspect ratio of $R_{45}/L=0.193$ (b), 0.235 (c), 0.309 (d), and 0.413 (e). For a definition of R_x, R_y, and R_{45} see inset of Fig. 2.

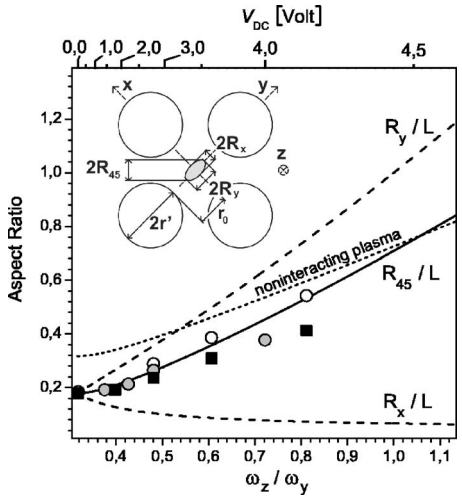

FIG. 2. Comparison of the aspect ratio R_{45}/L of a partially crystallized $^9Be^+$ plasma and the cold fluid prediction (solid and dashed lines) for zero-temperature ellipsoidal plasmas, as a function of the ratio ω_z/ω_y between the axial and the smallest transverse trap frequency. Full squares, large crystals from Fig. 1. Open (gray) circles, small (medium-size) crystals from Fig. 3. Dotted line, R_{45}/L for a low-density plasma in the gas phase with negligible particle interactions, where $R_x/L=\omega_z/\omega_x$, $R_y/L=\omega_z/\omega_y$. Inset, cross section of linear trap and of ellipsoidal plasma. Observation direction as in Fig. 1.

increase with the applied static quadrupole potential V_{DC}. There are several possible explanations for the observed structures. For nonzero V_{DC}, the cylindrical trap potential symmetry is broken. This induces changes in the shape and local order of the crystal, reducing the number of ion shells, as confirmed by the MD simulations. This effect is not directly related to temperature and increases with V_{DC}. Therefore, the CCD camera pictures which display the line-of-sight-integrated fluorescence of the ion crystal cannot resolve individual shells or ions in the inner region any more. Another contribution to the observed smearing of the crystal structure could originate from a larger average micromotion energy of the ions due to the crystal shape change which could lead to heating.

In contrast to the observation of large plasmas, we found that under similar laser-cooling parameters small plasmas containing only a few hundred $^9Be^+$ ions do not show a smeared-out core and could always be resolved by the CCD camera. However, these plasmas, see Fig. 3 and discussion below, are also consistent with the assumption of a larger average micromotion energy of particles in the outer shells of the crystal.

For all plasmas produced so far the ellipsoidal deformation is a reversible process if the maximum value of V_{DC} is kept within the range stated above: after turning V_{DC} off, the principal axes R_{45} and L of the crystal returned to the initial values, indicating that no ions were lost during deformation. The outer boundaries of the crystals in Fig. 1 can be well described by ellipses with the principal axes R_{45} and L. Since the CCD camera takes a projection along an axis at 45° with respect to the x and y axes, the principal axis R_{45} of each ellipse is related to the principal axes R_x and R_y of the corresponding ellipsoid by $R_{45}=[(R_x^2+R_y^2)/2]^{1/2}$. For the last crystal in the sequence, the boundary shows clear deviations from an ellipse; we attribute this to the presence of sympathetically cooled impurities of higher mass than $^9Be^+$, located at larger radii as compared to $^9Be^+$. The asymmetry along the trap axis is caused by cooling light pressure, which is not felt by the sympathetically cooled ions. In this case, the elliptical fit has been chosen to match the fragments of the outermost shell, which still exist at the left and right ends of the crystal.

Figure 2 shows a comparison between the measured aspect ratio R_{45}/L and the theoretical result from Eq. (2). The agreement between the experiment and the theory is good, considering that the $^9Be^+$ ion crystals did exhibit two phases and were not pure. In addition, a systematic deviation between the theory and the experiment is expected at the largest applied voltages V_{DC} because then the smallest ellipsoid dimension R_x becomes comparable to the shell spacing. In this limit, the cold fluid model continuum description is inaccurate.

The cold fluid model also determines the relative change of the crystal length $2L$ when V_{DC} is changed. For the actual trap settings $2L$ is expected to decrease to 83% from its initial value, when changing V_{DC} from 0 to 4.2 V. The length of the crystal in the last image in Fig. 1(e) is 84% of the initial one (a), which is in good agreement with the expected compression. Therefore, while at large V_{DC} the observed transverse crystal shape starts to deviate from the predictions

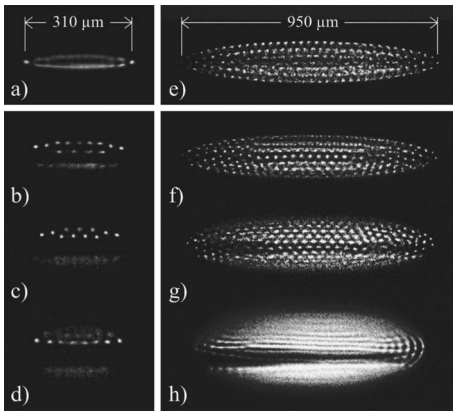

FIG. 3. Left, small crystal containing $\simeq 20\ ^9Be^+$ ions and a smaller number of sympathetically cooled impurity ions at different values of the static voltage V_{DC}: 0 V (a), 2.8 V (b), 3.6 V (c), and 4.2 V (d). Right, medium-size crystal containing $\simeq 500\ ^9Be^+$ ions. V_{DC} is set to 0 V (a), 1.4 V (b), 2.8 V (c), and 4.0 V (d). The asymmetric ion distribution in (b)–(d) and (f)–(h) is due to stray electric fields.

of the cold fluid model, the axial shape is still in good agreement since the axial dimension of the crystal remains large compared to the shell spacing.

While for the large Coulomb crystals a spatially averaged description is a good first approximation, in small crystals one may expect effects related to the particle structure to show up clearly. As an example, Figs. 3(a)–3(d) show a crystal containing about 20 $^9Be^+$ ions and several sympathetically cooled low-mass impurities. In an effective trap potential with cylindrical symmetry, the crystal exhibits a single $^9Be^+$ shell [Fig. 3(a)]. This shell appears smeared out in the CCD image (exposure time, 2 s), possibly because of a rotationlike diffusion of the ions around the trap axis. In the ellipsoidal crystals, Figs. 3(b)–3(d), this diffusion is suppressed because it would require overcoming an energy barrier, and therefore the image shows individual ions. The most apparent property arising when the static quadrupole voltage V_{DC} is increased is the completely dark region containing the sympathetically cooled particles. Furthermore, some of the fluorescence spots representing $^9Be^+$ ions, mainly those at larger distances from the trap center, appear smeared out and show a reduced intensity. We attribute this to heating induced by the micromotion occurring at the locations of these ions. As a test, we shifted the crystal by means of an additional static voltage applied to one trap electrode. This caused a rearrangement of the $^9Be^+$ relative to the dark core, but those ions that appeared well defined were always in the same region. However, for the static quadrupole voltages applied no ions are located in the front or the back of the dark region. Therefore, unlike for large ion crystals, we do not observe a smearing out of the crystal core as V_{DC} is increased.

Although the small crystals in Figs. 3(a)–3(d) do not exhibit closed boundaries, we could still fit ellipses to them. In order to compare such small crystals with the cold fluid model, half of the typical shell spacing of 29 μm was added to R_{45} and L before calculating the ratio R_{45}/L. The results are indicated by open circles in Fig. 2. Even for this case there is a good agreement with the cold fluid model. Finally, in Figs. 3(e)–3(h) we also present a medium-sized crystal containing $\simeq 500\ ^9Be^+$ ions and, again, additional low-mass impurities. The corresponding aspect ratio data as well as an additional data point for $V_{DC}=2.2$ V, reported in Fig. 2, also show good agreement with the theory. However, for large and medium-sized crystals a deviation between the theory and the experiment becomes obvious as the values for the static voltage V_{DC} increase. Our MD simulations show that the observed deviations can be explained by small ($<15\%$) admixtures of sympathetically cooled molecular impurities, in particular, H_2^+/H_3^+ ions close to the trap axis originating from residual gas contaminants and BeH^+ ions located in the outer regions of the crystals formed by chemical reactions.

The pronounced asymmetric ion distribution in the small, Figs. 3(a)–3(d), as well as in the medium-sized crystals, Figs. 3(e)–3(h), is not due to the broken cylindrical symmetry of the trap potential, as this does not produce any visible asymmetry in the CCD images. Instead, we attribute the asymmetric ion distribution to stray potentials. While it was not possible to compensate for these imperfections by additional static voltages, it was always possible to reverse the asymmetry by means of these voltages. Our MD simulations confirm this interpretation.

A direct estimate for the translational temperature of the Be^+ is obtained from the spectral line shape of its fluorescence as the cooling laser is tuned toward resonance and the ion ensemble crystallizes. Since the temperature of the particles changes during the frequency scan, we fit a Voigt profile to each point of the recorded fluorescence curve to determine an upper limit for the Be^+ temperature. For small crystals (<1000 particles), we find an upper limit for the temperature at the end of the scan of 42 mK. However, the accuracy of this method is limited due to the experimental resolution. An indirect upper limit is obtained by comparing the size of the ion spots with MD simulations, where we find a tighter limit of <10 mK for the Be^+ temperature. We deduce, assuming thermal equilibrium, that the temperature of the sympathetically cooled impurity ions in Fig. 3 is <10 mK.

VI. CONCLUSIONS AND OUTLOOK

In summary, we have studied the static behavior of Coulomb crystals in a fully anisotropic effective trap potential and found a good agreement with the simple cold fluid plasma model for small anisotropy. For larger anisotropy, deviations could be explained by the presence of additional, sympathetically cooled, ion species. From an experimental point of view, the ability to reversibly deform a crystal allows us to separate lower-mass sympathetically cooled ions from the laser-cooled ions. This allows us to obtain a clearer picture of the impurity ion ensemble, without any background or foreground fluorescence from the laser-cooled ions. It will also permit us to manipulate the sympathetically cooled ions in a more direct way. The ability to generate a variety of ellipsoidal crystals opens up several directions for further study, e.g., oscillation modes of such crystals and, in particular, the modes of two-species crystals. These modes could be of importance for identification of the nonfluorescent species. On the theoretical side, it is of interest to per-

form detailed studies of structures using the MD simulations, which are able to fully take into account the particle nature of the cold plasmas. As an example, our MD simulations have shown that in strongly squeezed ellipsoids ion rings can occur. These represent a novel low-dimensional structure whose detailed investigation should be of significant interest.

ACKNOWLEDGMENTS

The authors thank H. Wenz for the MD simulations. This work was supported by the Deutsche Forschungsgemeinschaft and the EU Network HPRN-CT-2002-00290 "Ultracold Molecules."

[1] R. C. Davidson, *Physics of Nonneutral Plasmas* (Imperial College Press, London, 2001).
[2] D. H. E. Dubin and T. M. O'Neil, Rev. Mod. Phys. **71**, 87 (1999).
[3] W. L. Slattery, G. D. Doolen, and H. E. DeWitt, Phys. Rev. A **21**, 2087 (1980).
[4] F. Diedrich, E. Peik, J. M. Chen, W. Quint, and H. Walther, Phys. Rev. Lett. **59**, 2931 (1987).
[5] M. G. Raizen, J. M. Gilligan, J. C. Bergquist, W. M. Itano, and D. J. Wineland, J. Mod. Opt. **39**, 233 (1992).
[6] M. Drewsen, C. Brodersen, L. Hornekær, and J. S. Hangst, Phys. Rev. Lett. **81**, 2878 (1998).
[7] M. D. Lukin, S. F. Yelin, and M. Fleischhauer, Phys. Rev. Lett. **84**, 4232 (2000).
[8] D. J. Berkeland, J. D. Miller, J. C. Bergquist, W. M. Itano, and D. J. Wineland, Phys. Rev. Lett. **80**, 2089 (1998).
[9] S. Schiller and C. Lämmerzahl, Phys. Rev. A **68**, 053406 (2003); S. Schiller and V. I. Korobov, *ibid.* **71**, 032505 (2005).
[10] Note, however, that λ_D can be comparable to or smaller than the plasma extension and the plasma can still be gaseous, i.e., $\Gamma < 2$. Such a plasma can still be described within the charged fluid model, as is the case for liquidlike plasmas, i.e., $\Gamma \geqslant 2$.
[11] L. Hornekær, N. Kjærgaard, A. M. Thommesen, and M. Drewsen, Phys. Rev. Lett. **86**, 1994 (2001).
[12] L. R. Brewer, J. D. Prestage, J. J. Bollinger, W. M. Itano, D. J. Larson, and D. J. Wineland, Phys. Rev. A **38**, 859 (1988).
[13] D. H. E. Dubin, Phys. Fluids B **5**, 295 (1992).
[14] X.-P. Huang, J. J. Bollinger, T. B. Mitchell, and W. M. Itano, Phys. Plasmas **5**, 1656 (1998).
[15] H. G. Dehmelt, Adv. At. Mol. Phys. **3**, 53 (1967).
[16] L. Turner, Phys. Fluids **30**, 3196 (1987).
[17] L. Hornekær, Ph.D. thesis, Aarhus University, 2000.
[18] T. Baba and I. Waki, Jpn. J. Appl. Phys., Part 1 **35**, L1134 (1996).
[19] H. Schnitzler, U. Fröhlich, T. K. W. Boley, A. E. M. Clemen, J. Mlynek, A. Peters, and S. Schiller, Appl. Opt. **41**, 7000 (2002).
[20] H. Wenz (private communication).
[21] B. Roth, U. Fröhlich, and S. Schiller, Phys. Rev. Lett. **94**, 053001 (2005).